

Provided for non-commercial research and education use.  
Not for reproduction, distribution or commercial use.



This article appeared in a journal published by Elsevier. The attached copy is furnished to the author for internal non-commercial research and education use, including for instruction at the authors institution and sharing with colleagues.

Other uses, including reproduction and distribution, or selling or licensing copies, or posting to personal, institutional or third party websites are prohibited.

In most cases authors are permitted to post their version of the article (e.g. in Word or Tex form) to their personal website or institutional repository. Authors requiring further information regarding Elsevier's archiving and manuscript policies are encouraged to visit:

<http://www.elsevier.com/copyright>



# Comparing the strength of f.c.c. and b.c.c. sub-micrometer pillars: Compression experiments and dislocation dynamics simulations

Julia R. Greer<sup>a,\*</sup>, Christopher R. Weinberger<sup>b</sup>, Wei Cai<sup>b</sup>

<sup>a</sup> Department of Materials Science, California Institute of Technology, Pasadena, CA 91125-8100, USA

<sup>b</sup> Department of Mechanical Engineering, Stanford University, Stanford, CA 94305-4040, USA

Received 23 February 2007; received in revised form 15 June 2007; accepted 7 August 2007

## Abstract

We compare mechanical strength of f.c.c. gold and b.c.c. molybdenum single crystal pillars of sub-micrometer diameter in uniaxial compression tests. Both crystals show an increase of flow stress with decreasing diameter, but the change is more pronounced in Au than in Mo. The ratio between the observed maximum flow stress and the theoretical strength is much larger in Au pillars than in Mo pillars. Dislocation dynamics simulations also reveal different dislocation behavior in these two metals. While in a f.c.c. crystal a dislocation loop nucleated from the surface simply moves on its glide plane and exits the pillar, in a b.c.c. crystal it can generate multiple new dislocations due to the ease of screw dislocations to change slip planes. We postulate that this difference in dislocation behavior is the fundamental reason for the observed difference in the plastic deformation behavior of f.c.c. and b.c.c. pillars.

© 2007 Elsevier B.V. All rights reserved.

**Keywords:** Dislocations; Nano-scale plasticity; Stress

## 1. Introduction

The strength of crystalline materials at the micro- and nano-scales is important for the fabrication and reliable functioning of devices at these scales. The plastic flow stress of crystals, a size-independent property for the bulk, is also found to depend on sample size as it is reduced to micro- and nano-scales [1–4]. Many models have been proposed to account for this size-dependence at small scales, including strain-gradient plasticity theories [5–12]. Recently, there has been much interest in micro-compression tests of cylindrical sub-micron pillars fabricated by the focused ion beam (FIB) method. The plastic flow stress increases dramatically as the diameter of the pillar decreases below 1  $\mu\text{m}$  [2,13,14]. This finding is interesting because it shows that the size effect can exist even without externally imposed strain gradients present in bending and indentation experiments. Several mechanisms have been proposed to explain the size effects in the micro-compression experiments [15,16]. We expect that dislocation dynamics (DD) simulations, when quantitatively compared with the experiments, will reveal the underlying mechanisms of this size dependence. DD simulations

were originally developed to model the plastic deformation of bulk crystals [17–20]. It has also been applied to thin films, in which we need to account for the effect of image stress on the dislocations due to the free surface [21,22]. We have recently developed an efficient method to compute the image stress in an elastic cylinder using a set of analytical solutions. This allows efficient DD simulations in micro-pillars. In this paper, we present the results of uniaxial compression of  $\langle 001 \rangle$  Au (f.c.c.) and Mo (b.c.c.) sub-micron pillars and compare them with DD simulations. The comparison reveals interesting differences in the dislocation dynamics in f.c.c. and b.c.c. pillars, and a possible explanation to the difference in the experimentally observed size effects on plasticity.

## 2. Experimental results

The pillars described in this work were fabricated via focused ion beam (FIB) and were subsequently uniaxially compressed along  $\langle 001 \rangle$  direction in the XP Nanoindenter. Gold pillars were fabricated from epitaxially grown thin films on MgO substrates while Mo pillars were machined from single crystal bulk sample. A representative Mo pillar (initial diameter = 830 nm) before and after compression is shown in Fig. 1. The final severe deformation state clearly shows that multiple slip systems were activated and that the compression was relatively homogeneous.

\* Corresponding author. Tel.: +1 626 395 4127; fax: +1 626 795 6132.  
E-mail address: jrgreer@caltech.edu (J.R. Greer).

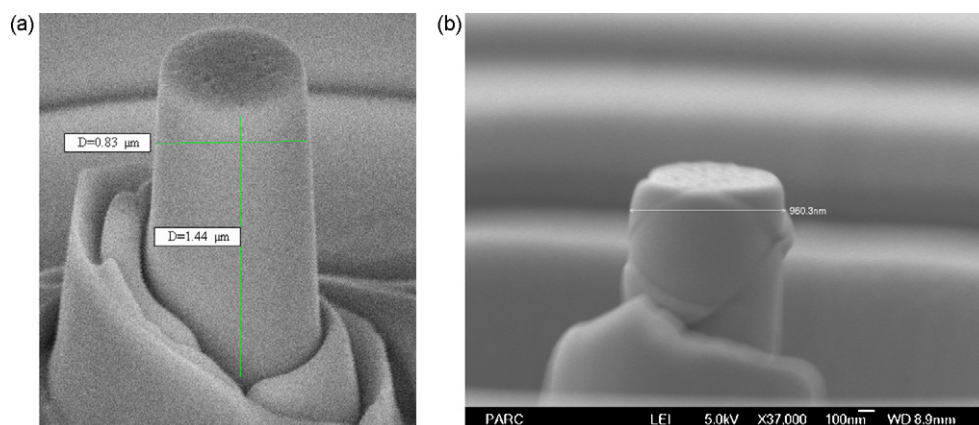


Fig. 1. A representative Mo (001)-oriented pillar before compression and after severe compression. Initial diameter ~830 nm, final diameter after compression ~960 nm.

Fig. 2 shows the true axial stress–strain curves generated based on the experimental load–displacement data collected by the Nanoindenter. The testing methodology and stress calculations are based on the authors’ previous work, which is fully described in Ref. [1]. The axial stress was calculated by dividing the imposed load by the plastic area determined based on conservation of volume during plastic deformation.

Some of the molybdenum pillars were compressed without intentional unloading in the middle of the experiment while the rest and all of the gold pillars were unloaded and re-loaded several times before reaching their final strain. All compression experiments were run in nominal constant displacement rate regime, corresponding to the nominal strain rate of  $3.33 \times 10^{-3} \text{ s}^{-1}$ . It is clear from the two sets of curves that at 10% strain, a 300-nm Mo nano-pillar reaches the stress of 2 GPa compared with 600 MPa for Au at equivalent strain. These nanopillars from both metals exhibit strengths much higher than their bulk equivalent, of ~450 MPa for Mo [24] and 25 MPa for Au [23]. The flow stress for bulk b.c.c. metals is much higher than that for bulk f.c.c. metals because of the higher lattice resistance to dislocation motion (e.g. Peierls stress) in b.c.c. metals. At the same time, density functional theory (DFT) predicts that the ideal shear strength of Mo on its slip plane is 15 GPa and that for Au is 850 MPa [25], which translates into

38 and 1.8 GPa ideal axial strength for Mo and Au, respectively. The axial stress was calculated from the ideal shear strength by dividing the latter by the Schmid factor for the slip systems considered in the ideal shear strength calculation:  $\{1 \bar{1} 0\}/(1 1 1)$  for the b.c.c. and  $\{1 1 1\}/(1 1 \bar{2})$  for the f.c.c. structure. The estimated axial strength will not change appreciably if we take a different slip system considered in Ref. [25], which will have a slightly different ideal shear strength and Schmid factor. These ideal axial strengths are shown as dashed lines in Fig. 2 for comparison.

From the above analysis, the 300-nm Au pillar achieves 33.5% of its theoretical strength while the 300-nm Mo pillar (the smallest and strongest in our experiment) reaches only 5.1% of its theoretical strength. Due to possible slight misalignment in the initial stages of deformation, we chose to compare flow stresses at 10% strain, when full contact is established, rather than yield stresses, which cannot be unambiguously defined here. Fig. 3 shows the size effects in Au and Mo pillars in terms of the flow stress at 10% strain versus pillar diameter. Half-filled symbols correspond to the experimental data taken in this work. Previously published Au micro-compression data of Greer and Nix [2] (filled circles) and a straight line that fits the data of Volkert and Lilleodden at 5% strain [14] are also shown for comparison. The data presented in this paper fits well within the

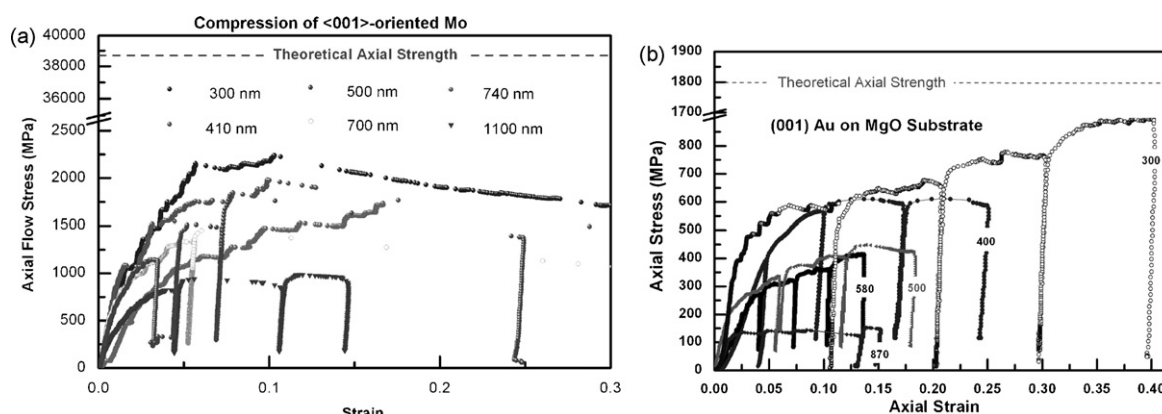


Fig. 2. Stress vs. strain for (a) b.c.c. Mo and (b) f.c.c. Au nano-pillars. Some Mo and all Au pillars were intentionally unloaded and re-loaded several times throughout the experiment. Numbers adjacent to each curve represent the initial diameter of the pillar.

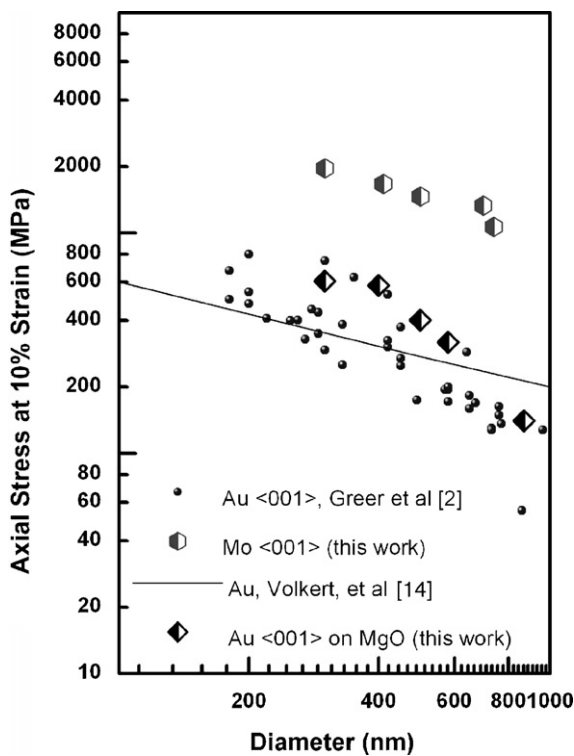


Fig. 3. Flow stress at 10% strain vs. size (diameter) for Au (f.c.c.) vs. Mo (b.c.c.). Half-filled symbols represent the experimental data from this work. Filled circles correspond to the (001)-oriented single crystal gold data of Greer and Nix [2], and straight line indicates the dependence found by Volkert and Lilleodden [14] for low-symmetry oriented pillars at 5% strain.

distribution of the previously published data by the author. The size effect in Au observed by Volkert and colleagues appears to be smaller, most likely due to the low-symmetry orientation of their pillars, which leads to inhomogeneous deformation. To our knowledge, no size effect data on homogeneous compression of b.c.c. samples has been published. Fig. 3 shows that the size effect on flow stress is more pronounced in Au pillars than in Mo pillars. As the pillar diameter decreases from 800 to 300 nm, the flow stress in Au pillars increase by more than a factor of 4, but the flow stress in Mo only increase by a factor of 2. This suggests that different dislocation mechanisms might be operating in f.c.c. and b.c.c. pillars. To gain further insights into the origins of this difference, we perform DD simulations in elastic cylinders with dislocations described by different mobility functions to mimic their behavior in f.c.c. and b.c.c. metals.

### 3. Modeling methods

The method of dislocation dynamics (DD) has been developed to track the time evolution of dislocation structures under external loading in order to link the physics of dislocation motion to the observed crystal plasticity. In these simulations dislocations are represented by discrete line segments connecting a set of nodes that move in response to the local Peach–Koehler forces, which arise from the applied loads and from interactions with other dislocations [26–29]. Dislocation velocities are computed from the forces using a mobility function that is

constructed based on the atomistic simulation results or experimental measurements. The DD simulations in this work are performed based on the ParaDiS code developed at Lawrence Livermore National Laboratory [28,29].

When modeling bulk crystals, the DD simulation cell is usually subjected to periodic boundary conditions (PBC) in all three directions. However, to apply DD simulations to small structures such as a micro-pillar, the effect of the free surfaces must be accounted for. This requires two important modifications to the existing DD method: the computation of image stress and the handling of the topology for a dislocation line intersecting a pillar surface. The image stress, originally discussed by Eshelby [30], is the difference between the stress state in an infinite body and that of the finite body containing the same arrangement of dislocations. The stress fields of dislocations can be readily computed in an infinite (isotropic) elastic medium but they require a set of traction forces  $\mathbf{T}$  at the surface when applied to a finite elastic medium such as a cylinder. The image stress is the stress field response of a defect-free cylinder subjected to a set of surface tractions that exactly cancels  $\mathbf{T}$ . A new method for computing the image stress in an isotropic elastic cylinder has been developed that takes advantage of the existence of analytic solutions in the Fourier space [31]. This method not only allows us to compute the image stress field at a point, but also gives analytical expressions for the integral of this stress field along another straight dislocation segment, facilitating the calculation of nodal forces in DD simulations.

DD simulations need to handle topological changes of the dislocation line network in order to capture the physics of junction formation and dissociation, dislocation annihilation, as well as to improve the discretization of the network by re-meshing. A simple but very general set of rules has been discussed in Ref. [29], in which two operations, node merge and node split, can be combined to capture all dislocation reactions in the bulk. However, these rules need to be extended to account for the intersection of dislocations with free surfaces. When a dislocation line intersects the surface, we place a node on the surface and continue the dislocation line outside the cylinder. This node is now constrained to move on the surface only, while the dislocation line outside the cylinder re-enters the cylinder at another node, where another dislocation segment intersects the surface. This is possible because the intersection points between dislocation line and the surface always form in pairs, when a dislocation half loop exits the surface. The continuation of the loop outside the cylinder is necessary since the expressions for dislocation stress field in the infinite medium are only valid for complete loops. The simulation results do not depend on the arrangement of the dislocation lines outside the cylinder as long as the Burgers vector is conserved everywhere, i.e. the dislocation line never ends by itself. The dislocation lines outside the cylinder are not shown in Figs. 4 and 5.

### 4. Modeling results

In order to gain a qualitative comparison of dislocation behavior in f.c.c. and b.c.c. pillars we performed DD simulations of glide loops in both crystal systems. The initial conditions are

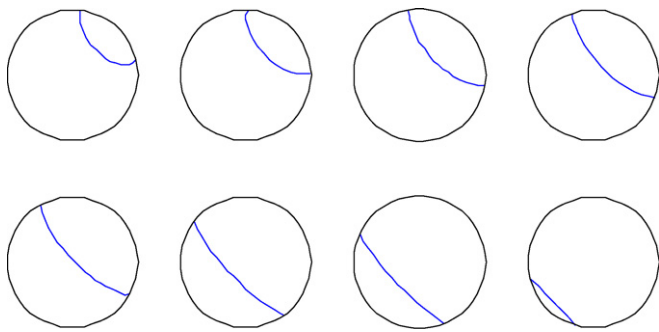


Fig. 4. Dislocation gliding along  $(1\ 1\ 1)$  plane in an f.c.c. Crystal (viewing along the cylinder axis). f.c.c. dislocations quickly escape to the surface leaving a dislocation starved cylinder.

small glide loops placed on the preferred glide planes  $(1\ 1\ 1)$  for the f.c.c. and  $(0\ \bar{1}\ 1)$  for the b.c.c. structure. The cylinder, whose axis is along the  $[00\ 1]$  direction, is subjected to uniaxial compression along this axis at a constant strain rate. The simulation strain rate is several orders of magnitude higher than that in the experiments. Its actual value is inconsequential here because we are also using generic values for the dislocation mobility. Scaling the dislocation mobility amounts to a rescaling of the time axis, which affects the strain rate. The main difference in the f.c.c. and b.c.c. simulations lies in the specification of the mobility function. In the f.c.c. model, the dislocation line is constrained to move in its glide plane. This reflects the fact that dislocations in f.c.c. metals dissociate into partial dislocations bounding a stacking fault ribbon which confines the motion of dislocations into a plane. This is an approximation because it suppresses the rare event of cross-slip in f.c.c. metals. In the b.c.c. model, screw dislocations are allowed to move in any plane that contains the Burgers vector. Both of these mobility laws are explicitly described in Ref. [33]. In the f.c.c. model, the edge and screw dislocations have the same mobility, while in the b.c.c. model, the edge dislocation segments move 10 times faster than the screw segments, when subjected to the same Peach–Koehler force.

Figs. 4 and 5 show sequential snapshots of a single dislocation loop moving through f.c.c. and b.c.c. pillars as viewed along the cylinder axis. The dislocation in the f.c.c. crystal sweeps across the plane quickly and exits the cylinder as expected. This is used

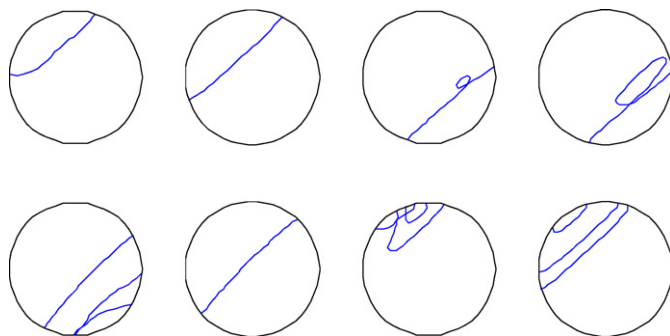


Fig. 5. Dislocation gliding along  $(0\ \bar{1}\ 1)$  plane in a b.c.c. pillar. The b.c.c. dislocation orients as a screw and emits additional dislocations promoting strain hardening.

in the “dislocation-starvation” model to argue that the cylinder needs to repeatedly nucleate dislocation loops from the surface in order to sustain the applied strain rate. In the b.c.c. crystal, the edge components exit the cylinder much faster, leaving behind a slower, largely screw oriented dislocation in the cylinder, which eventually sweeps across the slip plane. The motion of the screw dislocation closely follows the original  $(0\ \bar{1}\ 1)$  plane. As the dislocation approaches the other side of the cylinder, it forms a cusp because the dislocation line at the two sides of the cusp are not precisely positioned on the same plane. The cusp eventually develops into a loop, which then forms a new screw dislocation moving in the opposite direction as the original dislocation. When this dislocation approaches the surface, a similar scenario re-appears. But this time, it ends up sending three new dislocations in the opposite direction. The qualitative behavior reported here is robust against modification of simulation details such as the discretization length of dislocation segments. In bulk b.c.c. metals, screw dislocations are known to generate debris loops during motion [32]. This is due to the ability of the screw dislocation to move on any of the  $\{1\ 1\ 0\}$  planes that intersects the Burgers vector. It is likely that this process is enhanced by the image stress of the cylinder. Further analysis reveals that the image stresses near the two intersection points bias the dislocation motion in opposite directions which enhances the chance of cusp and loop formation. This is consistent with the observation that the loop formation always occurs when the dislocation gets close to the opposite surface.

Therefore, our DD simulations suggest that, when a new dislocation loop nucleates from the surface, its lifetime in a b.c.c. pillar is longer than that in an f.c.c. pillar. It may be able generate new dislocations on its own. Because the pillar is oriented for multi-slip, dislocation loops on different glide planes can nucleate and potentially intersect each other if they stay inside the pillar long enough. A longer residence lifetime for dislocations in b.c.c. pillars thus enhances the chances for junction formation and conventional strain-hardening by forest dislocations. We postulate that, because of this mechanism, the plastic deformation of b.c.c. pillars (with diameter at 300–800 nm) follow more closely the conventional model of forest hardening, than the dislocation starvation model, which seems to be more consistent with the observed behavior of f.c.c. pillars. We are currently performing DD simulations of multiple dislocation loops and cross-sectional TEM analysis for both f.c.c. and b.c.c. crystals to verify this hypothesis.

## 5. Conclusions

We investigated the stress–strain behavior of Au (f.c.c.) and Mo (b.c.c.) sub-micrometer pillars in uniaxial compression. Both types of crystals exhibit a strong size effect, with the relative strength change in gold being nearly twice compared to that of molybdenum over the same diameter range. We hypothesize that this difference is due to the difference in dislocation behavior between the two types of crystals, as suggested by our DD simulations. In f.c.c. crystals, the extremely high mobility of gliding dislocations makes their mutual interactions unlikely, which leaves the crystal dislocation-starved, requiring higher

stresses to nucleate new defects. In b.c.c. crystals, however, the dislocation residence time inside the crystal is relatively long, and the image stresses seem to enhance a dislocation's affinity for self-replication when it approaches a free surface. The entanglement of these dislocation segments inside the pillar can contribute to increased flow stress, similar to the forest-hardening model that describes the plasticity of bulk crystals. This suggests that the dislocation starvation model may not apply to b.c.c. pillars at the diameters considered in this study (300–800 nm). TEM images and further simulations and analysis are underway for a more thorough investigation on this topic.

## References

- [1] J.R. Greer, W.C. Oliver, W.D. Nix, *Acta Mater.* 53 (2005) 1821–1830.
- [2] J.R. Greer, W.D. Nix, *Phys. Rev. B* 73 (2006) 245410.
- [3] B. Wu, A. Heidelberg, J.J. Boland, *Nat. Mater.* 4 (2005) 525–529.
- [4] L. Nicola, Y. Xiang, J.J. Vlassak, E. Van der Giessen, A. Needleman, *J. Mech. Phys. Solids* 54 (2006) 2089–2110.
- [5] W.D. Nix, H. Gao, *J. Mech. Phys. Solids* 46 (1998) 411.
- [6] N.I. Tymiak, D.E. Kramer, D.F. Bahr, T.J. Wyrobek, W.W. Gerberich, *Acta Mater.* 49 (2001) 1021.
- [7] H. Gao, Y. Huang, W.D. Nix, *Naturwissenschaften* 86 (1999) 507.
- [8] H. Gao, Y. Huang, W.D. Nix, J.W. Hutchinson, *J. Mech. Phys. Solids* 47 (1999) 1239.
- [9] Y. Huang, H. Gao, W.D. Nix, J.W. Hutchinson, *J. Mech. Phys. Solids* 48 (2000) 99.
- [10] Y. Huang, Z. Xue, H. Gao, W.D. Nix, Z.C. Xia, *J. Mater. Res.* 15 (2000) 1786.
- [11] Y. Huang, J.Y. Chen, T.F. Guo, L. Zhang, K.C. Hwang, *Int. J. Fract.* 100 (1999) 1.
- [12] J.G. Swadener, E.P. George, G.M. Pharr, *J. Mech. Phys. Solids* 50 (2002) 681.
- [13] M.D. Uchic, D.M. Dimiduk, J.N. Florando, W.D. Nix, *Science* 305 (2004) 986–989.
- [14] C.A. Volkert, E.T. Lilleodden, *Phil. Mag.* 86 (2006) 5567.
- [15] J.R. Greer, *Rev. Adv. Mater. Sci.* 13 (2006) 59–70.
- [16] H.A.W. Ngan, P.C. Wo, L. Zuo, H. Li, N. Afrin, *Int. J. Mod. Phys. B* 20 (2006) 3579–3586.
- [17] B. Devincre, L.P. Kubin, *Mater. Sci. Eng. A* 8 (1997) 234–236.
- [18] K.W. Schwarz, *J. Appl. Phys.* 85 (1999) 108.
- [19] N.M. Ghoniem, L.Z. Sun, *Phys. Rev. B* 60 (1999) 128.
- [20] W. Cai, V.V. Bulatov, T.G. Pierce, M. Hiratani, M. Rhee, M. Bartelt, M. Tang, *Solid Mechanics and its Applications*, vol. 115, Kluwer Academic Publishers, Dordrecht, 2004, p. 1.
- [21] D. Weygand, L.H. Friedman, E. Van der Giessen, A. Needleman, *Model. Simul. Mater. Sci. Eng.* 10 (2002) 437–468.
- [22] D. Weygand, L.H. Friedman, E. Van der Giessen, A. Needleman, *Mater. Sci. Eng. A* 309/310 (2001) 420–424.
- [23] E.M. Savitskii, A. Prince, *Handbook of Precious Metals*, 1969, p. 128.
- [24] F. Guiu, P.L. Pratt, *Phys. Status Solidi* 15 (1966) 539.
- [25] S. Ogata, J. Li, N. Hirotsaki, Y. Shibutani, S. Yip, *Phys. Rev. B* 70 (2004) 104104.
- [26] K.W. Schwarz, *Phys. Rev. Lett.* 91 (2003) 145503.
- [27] N.M. Ghoniem, X. Han, *Phil. Mag.* 85 (2005) 2809–2830.
- [28] V.V. Bulatov, W. Cai, J. Fier, M. Hiratani, T. Pierce, M. Tang, M. Rhee, K. Yates, A. Arsenlis, *Proceedings of the ACM/IEEE Super Computing 2004 Conference (SC'04)*, 2004, p. 19.
- [29] A. Arsenlis, W. Cai, M. Tang, M. Rhee, T. Opperstrup, G. Hommes, T.G. Pierce, V.V. Bulatov, *Model. Simul. Mater. Sci. Eng.* 15 (2007) 553–595.
- [30] J.D. Eshelby, in: F.R.N. Nabarro (Ed.), *Dislocations in Solids*, vol. 1, North Holland Publishers, 1979, p. 167.
- [31] C.R. Weinberger, W. Cai, *J. Mech. Phys. Solids*, 2007.
- [32] J. Marian, W. Cai, V.V. Bulatov, *Nat. Mater.* 3 (2004) 158.
- [33] W. Cai, V.V. Bulatov, *Mater. Sci. Eng. A* 387–389 (2004) 277.